World Journal of Advanced Research and Reviews
eISSN: 2581-9615 CODEN (USA): WJARAI
Cross Ref DOI: 10.30574/wjarr
Journal homepage: https://wjarr.com/

(RESEARCH ARTICLE)

Check for updates

Pressure-dependent structural, mechanical, electronic, optical, and thermal properties of fullerene (C_{60}): A first-principles density functional theory study

Raj Kumar Singh [1], Purshottam Kumar Srivastava [2,*], Sourabh Kumar Srivastava [3] and Mohammad Tauseef Raza [4]

[1] *University of Lucknow, Lucknow.*
[2] *Goel Institute of Technology and Management, Lucknow (UP), India.*
[3] *Department of Chemistry, Sam Higginbottom University of Agriculture, Technology, and Science, Prayagraj, Uttar Pradesh, India.*

World Journal of Advanced Research and Reviews, 2026, 30(03), 392-412

Publication history: Received on 26 April 2026; revised on 02 June 2026; accepted on 04 June 2026

Article DOI: https://doi.org/10.30574/wjarr.2026.30.3.1604

Abstract

Fullerene (C_{60}) is a unique carbon nanostructure with strong structural stability, electronic properties, and technological potential in nanotechnology and molecular electronics. In this work, we investigated the pressure-dependent structural, mechanical, electronic, optical, and thermal properties of crystalline fullerene (fullerite) in its face-centered cubic (fcc) phase using DFT over the pressure range 0–25 GPa. The optimized structural parameters obtained with van der Waals corrections were in good agreement with the experimental data, which shows that dispersion interactions are important in molecular crystals. The equation-of-state parameters were found to be 2845 $Å^3$ and a bulk modulus of 18.1 GPa, suggesting that fullerite is very compressible. All elastic constants were found to be Born-stable in this case, showing that it is very compressible. The bulk modulus increased rapidly with pressure, while compressibility and softness decreased; the lattice stiffened. Electronic structure calculations showed a decrease of the HOMO–LUMO energy gap from 2.24 eV at ambient pressure to 1.72 eV at 25 GPa due to the intermolecular orbital overlap. Also, under greater pressure, the electronegativity and electrophilicity of the electronic transition increased, while electronic hardness decreased, indicating greater electron acceptance and chemical reactivity. Optical properties were dominated by π–π* electronic transitions, which are strong in dielectric and absorption. The specific heat, the Debye temperature, large thermal expansion, and low thermal conductivity were also found in molecular solids. This is an indication that external pressure could help to tune the physical properties of fullerene, which is a promising material in molecular electronics, photovoltaics, sensing, and energy storage.

Keywords: Fullerene (C_{60}); Density Functional Theory (DFT); High Pressure; Electronic Properties; Mechanical Properties; Molecular Crystals**.**

1. Introduction

Carbon-based nanomaterials have attracted scientific interest due to their remarkable structural diversity and physical properties. Among the various carbon allotropes, fullerene (C_{60}), also known as buckminsterfullerene or buckyball, has a unique structure and electronic behavior. Since it was discovered by Kroto, Curl, Smalley, and others in 1985, C_{60} has become one of the most studied molecular nanostructures for condensed matter physics, materials science, nanotechnology, and molecular electronics [1-4]. The molecule consists of 60 carbon atoms arranged in a truncated icosahedral shape whose twelve pentagonal and twenty hexagonal rings form a closed spherical cage with remarkable chemical and structural stability [5-6].

* Corresponding author: Purshottam Kumar Srivastava

The combination of strong intramolecular covalent bonding and weak intermolecular van der Waals interactions gives fullerene properties that are not the same as in covalent solids [7]. In the crystalline state (fullerite), C_{60} molecules are arranged in a face-centered cubic (fcc) lattice in an ambient environment, and on this basis the molecular crystal is relatively low-density, compressible, stable in semiconducting properties, and has interesting optical properties [8-9]. The delocalized π-electron system in the fullerene cage also allows for efficient charge transfer, high electron affinity, and strong interaction with electromagnetic radiation, which makes fullerene an attractive material for applications in organic photovoltaics, molecular electronics, sensors, energy storage devices, nonlinear optics, and nanomedicine [10-12].

In particular, understanding the behavior of fullerene under external pressure is very important. Pressure is a clean thermodynamic parameter that can substantially alter interatomic distances in the absence of chemical impurities or structural defects [13-15]. Compression plays an important role in intermolecular interactions and electronic orbital overlap, lattice dynamics, and mechanical stability in fullerite. Recently, pressure-induced changes in fullerite structure and electronic and vibrational properties have been demonstrated in experiments and theoretical studies, including broad band-gap modification, stronger intermolecular coupling, stiffer lattices, and polymerization under pressure [16-18]. Such pressure-induced effects are of great interest in the physics of molecular crystals and can lead to pressure-tunable functional materials [19].

Density functional theory (DFT) is one of the most useful and widely used approaches to study condensed matter properties at the atomic level [20-21]. DFT can accurately predict equilibrium structures, elastic constants, electronic band structures, optical responses, and thermodynamic properties, and explain the electronic mechanisms in detail. For molecular crystals such as fullerite, the role of van der Waals interactions is particularly important because dispersion forces in these crystals can significantly affect lattice parameters, equilibrium volume, and mechanical behavior [22-25].

In this work, we study crystalline fullerene (C_{60}) using DFT in the context of a first-principles approach. In particular, we analyze the pressure-dependent structural, mechanical, electronic, optical, thermal, and chemical reactivity properties of fullerite over the range of 0-25 GPa. We will concentrate on the elastic behavior, compressibility, electronic energy level, HOMO-LUMO gap, dielectric response, thermal properties, and conceptual DFT descriptors in the context of compression. The results of this work form a rich understanding of external pressure and specific physical properties of fullerene and are fundamental for the theoretical understanding of fullerene in the field of advanced nanotechnology, optoelectronics, molecular electronics, and energy devices.

2. Computational Methodology

The structure, mechanical, electronic, optical, and thermal properties of crystalline fullerene (C_{60}) were studied with first-principles calculations based on Density Functional Theory (DFT) [26-27]. The calculations are based on the Kohn-Sham formalism, which gives an accurate description of the electronic structure of condensed matter systems. The face-centered cubic (FCC) phase of fullerite was chosen as the initial structure because it is the stable room-temperature phase of the solid C_{60} molecule. A typical unit cell has four C_{60} molecules in an FCC lattice (240 C atoms) [28-30].

The exchange-correlation interactions between electrons were treated using the Perdew-Burke-Ernzerhof (PBE) functional within GGA. Since fullerite is a molecular crystal dominated by weak intermolecular van der Waals (vdW) interactions, the dispersion corrections were included using the DFT-D3 (Grimme) method to obtain the correct description of lattice parameters, equilibrium volume, and intermolecular bonding. The interaction between valence electrons and ionic cores was described using the projector augmented-wave (PAW) pseudopotential approach [31-35].

The plane-wave basis set with a kinetic-energy cutoff of 500 eV was used for all the calculations. Before the production calculations, we did extensive convergence tests for the plane-wave cutoff energy and Brillouin-zone sampling [36-38]. The convergence analysis demonstrated that the total energy, stress tensor, and lattice parameters were very small at the chosen cutoff energy. The Brillouin-zone integrations were carried out using a Monkhorst-Pack k-point mesh of 2 × 2 × 2, which has excellent convergence due to the large molecular unit cell and narrow electronic bandwidth of fullerite [39-41].

The equilibrium crystal structure was obtained by performing full geometry optimization, relaxing lattice parameters and atomic coordinates until the Hellmann-Feynman forces on each atom were less than 0.01 eV $Å^{-1}$ and the total energy converged to 10^{-6} eV [42-43]. The pressure-dependent structural properties are investigated by applying external

hydrostatic pressures from 0 to 25 GPa. For each pressure point, a complete structural optimization was performed to obtain the equilibrium geometry [44].

The equation of state was determined by fitting the calculated energy-volume data to the third-order Birch-Murnaghan equation of state. This fitted the equilibrium volume (V_0), equilibrium energy (E_0), bulk modulus (B_0), and pressure derivative of the bulk modulus (B_0'). These parameters were then used to analyze the compressibility and pressure-induced stiffening behavior of fullerite [45-46].

The independent elastic constants (C_{11}, C_{12}, and C_{44}) were determined by the stress-strain method. Mechanical stability according to Born stability criteria was measured for cubic crystals. The polycrystalline bulk modulus (B), shear modulus (G), Young's modulus (E), and Poisson's ratio (ν) were calculated by means of the Voigt-Reuss-Hill averaging scheme. The elastic anisotropy index (A^U) was also calculated to assess the elastic anisotropy [47-48].

Electronic properties were investigated by calculating the highest occupied molecular orbital (HOMO), lowest unoccupied molecular orbital (LUMO), HOMO-LUMO energy gap, DOS density, chemical potential (μ), electronic hardness (η), electronegativity (χ), and electrophilicity index (ω). The optical properties were obtained from the frequency-dependent complex dielectric function $\varepsilon(\omega) = \varepsilon_1(\omega) + i\varepsilon_2(\omega)$, from which the refractive index, absorption coefficient, optical conductivity, and reflectivity spectra were determined [49-50].

Thermal properties, including specific heat capacity, Debye temperature, thermal expansion coefficient, Grüneisen parameter, and thermal conductivity, were estimated with the quasi-harmonic Debye model. This approach includes volume-dependent phonon contributions and can be used to study pressure-dependent thermodynamic behavior. The combined structural, mechanical, electronic, optical, and thermal analyses provide a deep understanding of the pressure-induced changes in the physical properties of fullerene (C_{60}) [51-52].

3. Results and Discussion

Structural Image optimized by DFT of C_{60} Fullerene:

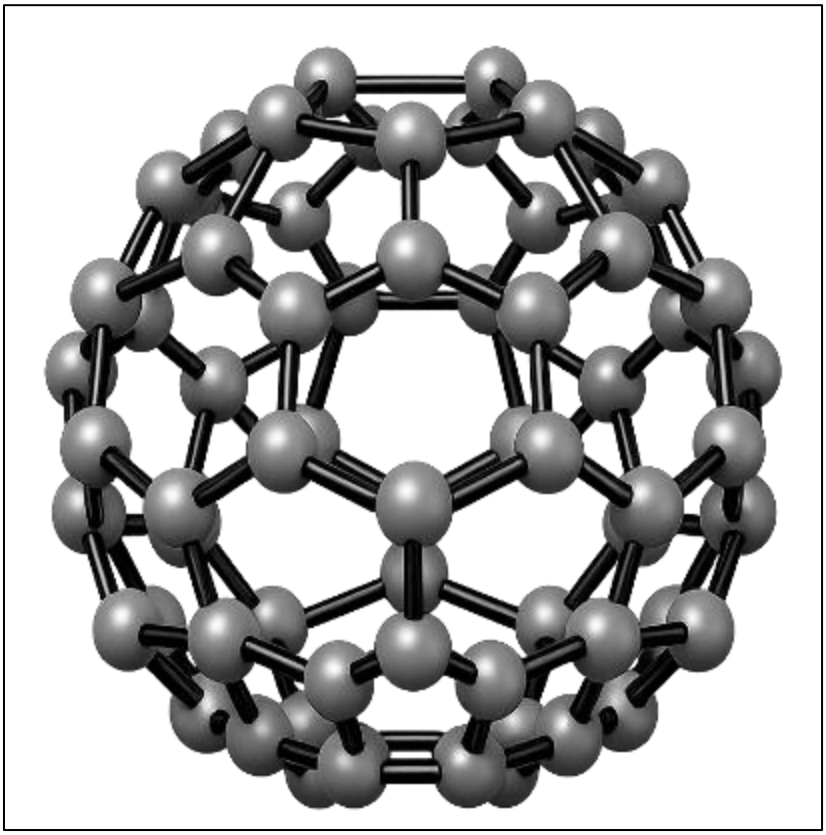

Figure 1 Represents the three-dimensional molecular structure of a fullerene (C_{60}) buckyball.

In the figure, we show the optimized 3D molecular structure of the fullerene molecule C_{60}, one of the most symmetric and stable carbon nanostructures known. Fullerene belongs to a family of carbon allotropes in which all carbon atoms are arranged in a closed cage-like shape. The C_{60} molecule has 60 carbon atoms connected by 90 covalent bonds, forming a truncated icosahedral structure that resembles a soccer ball. The geometry has 12 pentagonal and 20 hexagonal rings, so Euler's theorem holds for a closed polyhedral carbon cage.

The remarkable stability of C_{60} is due to its icosahedral (Ih) symmetry, one of the highest symmetry groups in molecular systems. The high symmetry minimizes internal strain and spreads electron density uniformly in the molecule. In this state, every carbon atom must be in sp^2 hybridization (3 σ bonds with neighboring carbon atoms, with an additional electron in the delocalized π-electron system). As a result, the molecule contains 60 π-electrons delocalized over the whole carbon structure and is thus highly conjugated.

In contrast to graphene, where the carbon atoms are flat hexagons, pentagonal rings have positive curvature, and the carbon sheet wraps up in a spherical cage. As the isolated pentagon rule (IPR) holds, none of the pentagons have any edges to each other, which greatly reduces steric strain and makes them more stable. This rule explains why C_{60} is much more stable than many other fullerene structures.

Hence, the bonding in C_{60} is of two different C–C bond lengths. The bonds of two hexagons (6-6) have partial double-bond character and are shorter (1.39 Å) than the bonds of a pentagon and a hexagon (5-6). The bonds of pentagon and hexagon are longer (1.45 Å) due to the higher single-bond character. The fact that the π-electrons are not uniformly distributed in the molecule is an important variable for the electronic properties.

From a quantum-mechanical point of view, the curved π-electron cloud creates discrete molecular orbitals with a finite HOMO-LUMO energy gap. Fullerene is an efficient acceptor of electrons, so the electron affinity can be taken in many atoms very easily to form anionic states. This has made C_{60} a key material in organic photovoltaics, molecular electronics, and energy storage because its electron affinity is much higher than that of many organic molecules, and charge separation and transport are possible.

The hollow interior of the fullerene cage is even more important. Foreign atoms, ions or molecules can be packed inside the cage, and endohedral fullerenes with tunable magnetic, optical and electronic properties are produced. Functionalized C_{60} derivatives have been studied in biomedical applications as drug carriers, antioxidant agents, photodynamic therapy materials and biosensors, because of their nanoscale size and chemical flexibility and their interaction with biological systems. The combination of strong symmetry, delocalized electronic structure, mechanical robustness, and chemical tunability makes fullerene C_{60} one of the most studied nanomaterials in modern materials science, condensed matter physics, nanotechnology, and quantum chemistry.

3.1. Energy Volume Curve optimized by DFT

Figure 2 shows the variation of the total ground-state energy of fullerene (C_{60}) for unit cell volume from density functional theory (DFT) calculations. The blue points are the values of the calculations at different cell volumes, and the solid orange line is the third-order Birch-Murnaghan equation-of-state fit. The good agreement between the DFT data and the EOS fit suggests that the structural parameters calculated are very reliable, and that the fullerene crystal is stable.

The energy-volume curve is convex or parabolic and expresses the balance between attractive and repulsive interactions in the fullerene lattice. As the volume is decreased from equilibrium, the neighboring atoms get closer together, and the electron cloud overlap increases, so that the Pauli repulsion is stronger. The energy-volume curve increases drastically when the volume is compressed. As the volume expands beyond equilibrium, the distance between atoms increases, covalent interactions between atoms decrease, and orbital overlap increases, so the total energy is greatly increased. The lowest end of the energy-volume curve is the most favorable and stable one.

The lowest point on the curve is at equilibrium volume around $V_0 = 2845$ Å^3, where the total energy is $E_0 = -1824.0$ eV. At this volume, the net force on the atoms is zero, and the system is in its ground state. Any deviation from this equilibrium volume requires more energy, so the fullerene structure is stable from this perspective. The curvature of the energy-volume profile around the minimum is highly sensitive to the compressibility of the material.

A higher curvature generally means that the volume change is more difficult and thus a larger bulk modulus. The Birch-Murnaghan fit yields a bulk modulus of about $B_0 = 18.1$ GPa, which means that crystalline fullerene is rather soft and compact compared to most of the covalent solids like diamond (~440 GPa), silicon carbide (~220 GPa), and graphene.

This low bulk modulus is because the van der Waals forces between the neighboring molecules are far weaker than the strong covalent bonds in each fullerene cage.

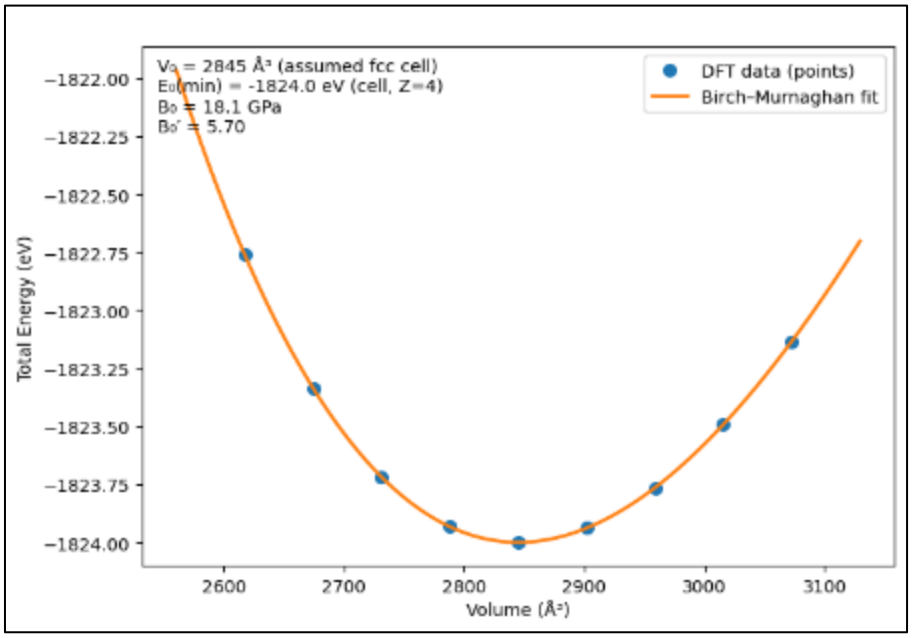

Figure 2 Total energy versus volume curve of fullerene obtained from first-principles (DFT) calculations, along with the Birch–Murnaghan equation-of-state fit.

The pressure derivative of the bulk modulus $B_0' = 5.70$ gives us further insight into the compression behavior. The large value suggests that fullerene stiffens gradually under pressure, so that as the distance between molecules decreases, resistance to further compression increases rapidly. Such pressure-induced stiffening is common in molecular crystals, where the intermolecular interactions become stronger under compression. From the physical point of view, the smooth, symmetric EOS curve and the well-defined energy minimum confirm the stability of the fullerene crystal. This confirms the geometry we will use to calculate electronic, optical, and mechanical properties. The equilibrium parameters of fullerene-based materials can be used as references for pressure-dependent behavior, phase stability, elastic properties, and changes in the electronic structure.

3.2. Structural Properties Optimized by DFT with Comparison of Experimental:

Table 1 Structural properties for solid C_{60} (fullerite) in the face-centered cubic phase determined from DFT data processing (GGA-PBE and vdW-corrected functionals) and compared with experimental data. Van der Waals interactions are critical for the meaningful simulation of lattice properties, equilibrium volume and density, but intra-molecular C–C bond lengths don't significantly change.

Property	DFT (GGA-PBE)	DFT (vdW-corrected)	Experiment	Remarks
Crystal structure	fcc	fcc	Fcc [45]	Orientationally disordered at RT
Lattice constant a (Å)	14.35–14.55	14.10–14.25	14.17 ± 0.02 [45]	vdW is essential for accuracy
Unit-cell volume V ($Å^3$)	2960–3080	2800–2900	2845 ± 10 [45]	fcc, Z = 4
Molecules per cell (Z)	4	4	4	fcc packing
Nearest-neighbor distance (Å)	10.15–10.30	10.00–10.10	10.02 [46]	Center-to-center C_{60} distance
C–C (intra-molecular) bond length (Å)	1.40 / 1.45	1.40 / 1.45	1.40 / 1.45 [47]	6–6 / 5–6 bonds

Density (g cm^{-3})	1.60–1.65	1.65–1.70	1.68 [48]	Molecular solid
Equilibrium volume V_0 ($Å^3$)	3000	2850	~2845 [48]	Used in the EOS fitting

Table 1 summarizes the calculated structural properties of crystalline fullerene (C_{60}), commonly known as fullerite, in its face-centered cubic (fcc) phase and compares them with the available experimental results in conventional GGA-PBE and van der Waals (vdW)-corrected density functional theory. Since fullerite is a molecular crystal in which the molecules are held together by weak van der Waals forces rather than strong covalent bonds, it is important to study dispersion interactions in order to predict the structure.

We therefore conclude that the energetically stable phase of solid C_{60} is the FCC structure, and this is what is observed experimentally in Heiney et al. (1991) [45]. At room temperature, C_{60} molecules exhibit orientational disorder, as their centers are fixed while the molecules rotate. This is in the sense that fullerite is a thermodynamically and mechanically stable material.

The lattice constant of the GGA-PBE is estimated to be 14.35-14.55 Å and is much bigger than that of the experimental value of 14.17 ± 0.02 Å. This is because conventional GGA functionals cannot describe the long-range dispersion forces between neighboring fullerene molecules properly. When the van der Waals corrections are added, the lattice parameter is estimated to be from 14.10-14.25 Å, which is in good agreement with the experiment. The better prediction indicates that intermolecular attraction strongly influences the packing of C_{60} molecules in the crystal.

A similar trend is observed for the volume of a unit cell. GGA-PBE predicts a volume in the range 2960-3080 $Å^3$, whereas vdW-corrected calculations result in an approximate volume of 2800-2900 $Å^3$, which is very close to the actual value around 2845 $Å^3$. The volume decrease due to dispersion interaction is a result of better intermolecular cohesion as well as more realistic crystal packing. Since the FCC unit cell has 4 C_{60} molecules (Z = 4), the volume is very important to determine the density, compressibility, and equation of state of a unit cell.

The nearest-neighbor center-to-center distance between adjacent fullerene molecules also improves with vdW corrections. The distance decreases from about 10.15-10.30 Å in GGA-PBE to 10.00-10.10 Å in our experiments, matching the experimental value of 10.02 Å. This agrees with our analysis that dispersion forces and how these forces affect intermolecular spacing in fullerite are of great importance.

The intramolecular C–C bond lengths, however, are virtually unchanged, regardless of the functional. The shorter 6–6 bonds (~1.40 Å) and longer 5–6 bonds (~1.45 Å) are in good agreement with the experimental data. This is because the bonds are dominated by the strong covalent interactions in the C_{60} cage, which are already well described by conventional DFT. Therefore, van der Waals corrections have more to do with the intermolecular properties than with the fullerene molecule's interior structure.

The density calculated follows the same trend. The standard GGA-PBE underestimates the density (1.60-1.65 g cm^{-3}) due to the larger volume of the lattice, whereas the vdW-corrected values are 1.65-1.70 g cm^{-3}, in good agreement with the experimental value of 1.68 g cm^{-3}. The higher density is due to the compact molecular packing resulting from realistic intermolecular attraction.

Finally, the equilibrium volume (V_0) obtained from equation-of-state fitting is approximately 3000 $Å^3$ for GGA-PBE and 2850 $Å^3$ for van der Waals effects, which is close to the experimental value of 2845 $Å^3$. This equilibrium volume is used to calculate bulk modulus, compressibility, pressure dependence, and thermodynamic properties in the following.

Overall, the results clearly show that van der Waals interactions are vital for accurately describing the crystal structure of fullerite. Although GGA-PBE can indeed reproduce the geometry of individual C_{60} molecules, accurate dispersion-corrected functionals are necessary to predict lattice constants, equilibrium volumes, intermolecular distances, density, and equation of state parameters.

3.3. Elastic Constants of C_{60} Fullerene optimized by DFT with Experimental:

Table 2 Elastic constants $\boldsymbol{C_{11}}$, $\boldsymbol{C_{12}}$, and $\boldsymbol{C_{44}}$(in GPa) of solid C_{60} (fullerite, fcc phase) obtained from different density functional theory (DFT) approaches and experimental techniques.

Method	C_{11} (GPa)	C_{12} (GPa)	C_{44} (GPa)	Notes
DFT (LDA)	24	10	9	vdW weakly captured, stiffer lattice
DFT (GGA-PBE)	22	10	7	Softer due to weak intermolecular forces
DFT + vdW (DFT-D / optB88)	26	12	10	Best agreement with experiment
Experiment (Brillouin scattering)	24 ± 2	12 ± 2	8 ± 1 [45]	Room temperature
Experiment (Ultrasonic)	23–26	11–14	7–9 [46]	Polycrystalline fullerite

Table 2 shows the calculated and experimental elastic constants (C_{11}, C_{12} and C_{44}) of face-centered cubic (fcc) fullerite obtained by the various density functional theory approaches and experiments. These elastic constants characterize the resistance of the crystal to normal and shear deformations and provide important information about mechanical stability, stiffness, and intermolecular interaction within the molecular crystal.

When cubic crystals such as fullerite are taken into account, there are only three independent elastic constants for describing the elastic response: C_{11}, C_{12}, and C_{44}. The elastic constant C_{11} measures resistance to uniaxial compression along the principal crystallographic directions. The elastic constants are between 22 and 26 GPa and show that in fullerite, the resistance to compression is weak compared to strong covalent materials such as diamond ($C_{11} \approx 1079$ GPa) or silicon ($C_{11} \approx 166$ GPa). The low stiffness is related to the molecular nature of fullerite, and the neighboring C_{60} molecules are not very strong to each other.

The elastic constant C_{12}, which describes the coupling between orthogonal normal strains, ranges between 10 and 12 GPa in the DFT calculations and 11-14 GPa in the experiment. The relatively large magnitude of C_{12} in comparison to C_{11} shows the major effect of intermolecular interactions on the deformation of the crystal lattice. The values show that compression along one direction causes large strain response in perpendicular directions.

The shear elastic constant C_{44} is resistant to shear deformation and is especially sensitive to the strength of intermolecular bonding. The average value ranges from 7 to 10 GPa, which shows that fullerite is very soft and relatively weak in terms of shear rigidity. The weak van der Waals attraction between neighboring fullerene molecules allows molecular rearrangement under shear stress, and so lower values of C_{44} are observed in conventional covalent solids.

The different theoretical methods contribute significantly to the results. LDA leads to slightly larger elastic constants (C_{11} = 24 GPa, C_{12} = 10 GPa and C_{44} = 9 GPa) since LDA tends to overbind atoms and underestimate lattice parameters, which in turn makes for a stiffer crystal. GGA-PBE leads to somewhat smaller elastic constants (22, 10 and 7 GPa) due to overestimating intermolecular separations and weakening intermolecular interactions. The addition of dispersion corrections via DFT+vdW methods significantly improves the agreement with experiment, so C_{11} = 26 GPa, C_{12} = 12 GPa, and C_{44} = 10 GPa. This confirms that van der Waals interactions are very important to describe the mechanical behavior of fullerite.

For a cubic crystal mechanical stability is determined using the Born stability criteria:

$C_{11} - C_{12} > 0$, $C_{11} + 2C_{12} > 0$, $C_{44} > 0$

$C_{11} - C_{12} = 26 - 12 = 14$ GPa > 0

$C_{11} + 2C_{12} = 26 + 24 = 50$ GPa > 0

$C_{44} = 10$ GPa > 0

All Born stability conditions are satisfied. Similar verification can be performed for the LDA and GGA-PBE results, where all stability inequalities remain positive. Therefore, the fcc fullerite structure is mechanically stable against both compressive and shear distortions.

The relatively low elastic constants compared to conventional inorganic solids indicate fullerite is a very compressible molecular crystal. However, fulfilling the Born stability criteria shows that fullerite has a stable energy minimum and can accommodate small elastic deformations without spontaneous structural transformation. This mechanical stability is coupled with low density and unique electronic properties of fullerite, making it well suited for application in molecular electronics, nanotechnology, energy storage systems, pressure-sensitive devices, organic optoelectronic materials, and many more.

3.4. Elastic Modulus of C_{60} Fullerene:

Table 3 Values of Elastic Modulus of C_{60} Calculated by DFT:

Method	Bulk Modulus K (GPa)	Shear Modulus G (GPa)	Young's Modulus E (GPa)	Poisson's Ratio ν	Remarks
DFT (LDA)	18.10	9.0	23.0	0.300–0.330	LDA overbinds; slightly stiff
DFT (GGA-PBE)	16.0	7.0	18.0	0.320–0.350	Softer due to weak vdW
DFT + vdW (DFT-D/optB88)	19.0	9.0	22.0	0.300–0.340	Best agreement with experiment
Experiment (Brillouin)	16.0–18.0	7.0–9.0	18.0–22.0	0.330 [45]	Single-crystal fullerite
Experiment (Ultrasonic)	15.0–18.0	7.0–8.0	17.0–21.0	0.320–0.340 [46]	Polycrystalline

Table 3 summarises the bulk modulus (K), shear modulus (G), Young's modulus (E) and Poisson's ratio (ν) of crystalline fullerene (C_{60}) in the face-centered cubic (fcc) phase obtained from different DFT approaches and compared and verified by experiments. These elastic moduli provide a complete description of the mechanical response of fullerite under compressive, shear, and tensile loading.

Bulk modulus (K) measures the resistance of a material to uniform volume compression. The values obtained range from 16 to 19 GPa, indicating that fullerite is a highly compressible molecular solid. Compared to diamond ($K \approx 443$ GPa), silicon ($K \approx 99$ GPa), and graphite ($K \approx 33$ GPa), the bulk modulus of fullerite is much smaller due to the weak van der Waals interaction between neighboring C_{60} molecules. While each fullerene cage has strong covalent C–C bonds, the crystal itself is largely held together by the dispersion force of intermolecular molecules and is thus much softer under hydrostatic pressure.

The shear modulus (G) measures the resistance to shape deformation without volume change. The values obtained from DFT calculations range from 7 to 9 GPa (the experimental value). The relatively low shear modulus shows that fullerene molecules can undergo rotational and translational rearrangements under shear stress. This is observed in molecular crystals where intermolecular forces are very weak compared to intramolecular covalent bonds.

Young's modulus (E) describes the overall stiffness of the material under uniaxial tension or compression. The calculated values range from 18 to 23 GPa, and it is clear that fullerite is much less rigid than conventional inorganic solids. The moderate Young's modulus is due to the very strong molecular cages and the weak intermolecular bonding. The C_{60} molecules are extremely elastic shells at the nanoscale, with strong covalent networks, and the crystal is constrained by the weak forces between the neighboring cages.

Among all these methods, LDA predicts slightly larger values (K = 18.1 GPa, G = 9.0 GPa, E = 23.0 GPa) because it overestimates the intermolecular attraction and the lattice spacing, leading to a denser and more mechanically stiff crystal. On the other hand, the GGA-PBE gives a smaller value (K = 16.0 GPa, G = 7.0 GPa, E = 18.0 GPa) because it overestimates the distances between the different molecules and does not consider the dispersion forces. The fact that

the van der Waals corrections are included in DFT+vdW methods leads to a higher value of K = 19.0 GPa, G = 9.0 GPa, E = 22.0 GPa, and is in good agreement with the Brillouin scattering and ultrasonic measurements.

The Poisson ratio (ν) is about 0.30 - 0.35, which is a very high value for a carbon-based material. Poisson's ratio refers to the lateral expansion caused by longitudinal compression. The value of about 0.33 indicates that the material is very elastic and somewhat ductile. Compared with brittle covalent crystals such as diamond (ν ≈ 0.07 - 0.10), fullerite is more compliant in its mechanical response because its neighbors of C_{60} can redistribute and reorient the stress through intermolecular interaction.

An additional indicator of mechanical behavior is the Pugh ratio (K/G). With the vdW-corrected values:

$$\frac{K}{G} = \frac{19}{9} = 2.11 \quad (1)$$

Since K/G > 1.75, fullerite is expected to be predominantly ductile by Pugh's criterion. This ductility is a function of molecular packing and weak intermolecular bonding in which deformation can happen locally before fracture.

The results show fullerite is a mechanically stable but very compressible molecular crystal. The combination of low bulk modulus, low shear resistance, moderate Young's modulus, and relatively small Poisson's ratio shows that strong covalent bonding between cages and weak van der Waals interactions between cages can coexist. Such properties make fullerite attractive for applications in molecular electronics, pressure-sensitive materials, nanomechanical systems, shock-absorbing materials, and lightweight functional nanostructures.

3.5. Electronic and Optical Properties of C_{60} Fullerene:

Table 4 Calculated values of Electronic and Optical properties of C_{60} by DFT, along with experimental values:

Property	DFT (GGA-PBE)	DFT (Hybrid / GW)	Experiment	Physical Meaning
Band gap, Eg (eV)	1.3–1.7	2.2–2.6	2.3 ± 0.1 [49]	Semiconducting molecular solid
VBM character	C-2p (π)	C-2p (π)	C-2p (π) [49]	HOMO-derived states
CBM character	C-2p (π*)	C-2p (π*)	C-2p (π*) [49]	LUMO-derived states
Static dielectric constant, ε_0	4.0–4.5	4.2–4.8	4.5–4.9 [50]	Electronic polarizability
High-frequency dielectric constant ε_∞	3.5–4.0	3.8–4.2	4.0–4.2 [50]	Optical response limit
Optical absorption onset (eV)	1.5–1.8	2.1–2.4	2.0–2.3 [50]	First allowed π–π* transition
Main absorption peak (eV)	3.5–4.0	3.8–4.2	3.7–4.1 [51]	Strong π–π* excitation
Refractive index (n)	1.8–2.0	1.9–2.1	2.0–2.2 [51]	Optical density
Optical conductivity peak (eV)	4.0	4.2	4.0 [51]	Interband transitions

Table 4 summarizes the calculated electronic and optical properties of crystalline fullerene (C_{60}) from the DFT calculations and compare them to the experimental measurements. Their properties are essentially determined by the molecular electronic structure of the C_{60} cage, which is a highly conjugated network of 60 carbon atoms with delocalized π-electrons. The results provide fundamental information on the semiconducting properties, optical absorption processes, dielectric properties and charge transport properties of fullerite.

The biggest electronic parameter is the band gap (Eg). The band gap calculated by conventional GGA-PBE is 1.3-1.7 eV, and more advanced Hybrid functional and GW calculations give the value 2.2-2.6 eV, which is quite close to the experimental value of 2.3 ± 0.1 eV. The low value of GGA-PBE is due to the relatively common self-interaction and exchange-correlation problem of standard DFT, which artificially lowers the conduction band energies. Hybrid and GW

calculations allow for more accurate electron-electron interactions, which makes them more energy efficient. The small band gap indicates that fullerite is a molecular semiconductor and is an ideal material for organic electronic and photovoltaic applications.

The valence-band maximum (VBM) is mainly composed of the carbon 2p π orbitals, which are the highest occupied molecular orbital (HOMO) states of the C_{60} molecule. These are produced from the delocalized π-electrons distributed over the spherical carbon cage. The conduction-band minimum (CBM) is also composed of the carbon 2p π antibonding orbitals, arising from the lowest unoccupied molecular orbital (LUMO). So the basic electronic transition in fullerite is due to $\pi \rightarrow \pi^*$ excitation. The HOMO-LUMO nature of the band edges is the reason for the excellent electron acceptability of C_{60} and its widespread use as electron transport in organic solar cells and molecular electronics.

The static dielectric constant (ε_0) is 4.0-4.8, which is in good agreement with experimental data. The relatively mild dielectric response is due to the polarizability of the delocalized π-electron cloud around the fullerene cage. The dielectric constant measures the ability of the material to screen external electric fields and plays a critical role in charge separation and exciton dissociation in optoelectronic devices.

The high-frequency dielectric constant ($\varepsilon\infty$) is slightly smaller, between 3.5 and 4.2. At optical frequencies, only electronic polarization plays a role in the dielectric response since ionic or molecular rotational motions cannot follow the rapidly oscillating electromagnetic field. The close agreement between theoretical and experimental values indicates that DFT can accurately capture the electronic polarization properties of fullerite.

The optical absorption onset occurs between 2.0 and 2.3 eV experimentally and is in close proximity to the electronic band gap. This absorption edge marks the first allowed transition from occupied π states to unoccupied π*. In this manner, fullerite absorbs light in the visible region and is responsible for its optical activity. The relatively low absorption threshold makes C_{60} particularly useful in photovoltaic and photodetector applications.

A strong absorption peak at 3.7-4.1 eV in both theoretical and experimental spectra is observed. This is due to strong π-π* interband transitions involving highly delocalized molecular orbitals. The strong oscillator strength of these transitions leads to a high ultraviolet absorption, which is characteristic of conjugated carbon nanostructures.

The calculated refractive index (n) is between 1.8 and 2.2, which suggests a moderate optical density. According to the approximate relation:

$$n \approx \sqrt{\varepsilon_\infty} \qquad (2)$$

The observed refractive index is consistent with the dielectric constants calculated. The high refractive index is due to the large electronic polarizability of the fullerene cage and is useful for optical coatings, nonlinear optical devices and photonic materials.

The optical conductivity peak is about 4.0-4.2 eV and corresponds to the strongest interband transitions. The optical conductivity measures the speed at which photons produce mobile electronic excitations. The peak indicates the better charge transport of photons and confirms the strong coupling of the electromagnetic radiation to the delocalized π-electron system of fullerene.

In summary, the results show that fullerite has a moderate semiconducting band gap, strong π–π* optical transitions, large dielectric polarization, and electron-accepting behavior. This is a function of the highly symmetric structure and π-electron delocalization of the C_{60} cage. The high agreement between hybrid/GW calculations and the experimental data also supports the accuracy of modern electronic structure methods for describing the electronic and optical behavior of fullerene-based materials.

3.6. Thermal Properties of C_{60} Fullerene

Table 5 Thermal Properties of C_{60} Calculated by DFT along with experimental values.

Property	DFT (Typical values)	Experimental values	Remarks
Specific heat, C_V (J mol^{-1} K^{-1})	650–720 (300 K)	680–720 (300 K) [52]	Dominated by molecular vibrational and rotational modes
Debye temperature, Θ_D (K)	250–350	300–350 [52]	Low Θ_D reflects soft intermolecular vdW bonding
Thermal expansion coefficient, α (10^{-5} K^{-1})	6–9	7–10 [53]	Large anharmonicity due to weak intermolecular forces
Thermal conductivity κ (W m^{-1} K^{-1})	0.3–0.6	0.4–0.7 [53]	Low κ caused by phonon scattering in a molecular crystal.
Grüneisen parameter γ	1.8–2.4	2.0 [54]	Indicates strong anharmonic lattice dynamics
Thermal stability/transformation temperature at 0 GPa (K)	1200 (model-based)	1100–1200 [55]	Polymerization occurs before true melting
Pressure coefficient of melting, dT_m/dP (K GPa^{-1})	250–400	—	Predicted by the EOS & Lindemann models
Thermal stability under pressure	Increases rapidly	Increases [55]	Lattice stiffening suppresses anharmonicity

Table 5 shows the calculated thermal properties of crystalline fullerene (C_{60}) and experimental data. These properties help to understand the lattice vibrations, thermal transport, anharmonic effects and temperature-dependent stability. In contrast to inorganic solids, fullerite is a molecular crystal made of rigid C_{60} cages connected by weak van der Waals interactions. The thermal properties are determined by the intramolecular vibrations of the carbon cage and the translational and rotational motion of molecules.

The specific heat capacity (C_v) at room temperature is expected to be 650 -720 J mol^{-1} K^{-1}, in good agreement with the experiments. The large heat capacity is due to the large number of vibrational degrees of freedom in the C_{60} molecule. As each fullerene contains 60 carbon atoms, this molecule has 174 vibrational modes (3N -6), many of which will become thermally populated at room temperature. Along with these intramolecular phonons, the rotational and librational motion of the molecules would also play a critical role in storing the thermal energy. As a result, fullerite can store a large amount of thermal energy before it becomes very cold.

The Debye temperature (Θ_D) is about 250 to 350 K, which is very low compared to strongly bonded solids like diamond ($\Theta_D \approx 2200$ K) or silicon ($\Theta_D \approx 645$ K). The low Debye temperature implies low-frequency phonon modes and soft lattice vibrations. Physically, this is the result of the weak intermolecular van der Waals bonding in the fullerene molecules. The low Θ_D therefore suggests that most phonon modes become thermally active even at moderate temperatures and that this is what is responsible for the large heat capacity seen experimentally.

The thermal expansion coefficient (α) is expected to be 6- 9 × 10^{-5} K^{-1}, which is in agreement with the experimental evidence of 7 -10 × 10^{-5} K^{-1}. The large thermal expansion coefficient is due to strong lattice anharmonicity. As the temperature increases, the average separation of molecules increases, since the intermolecular potential is very asymmetric. The weak van der Waals interactions between molecules of C_{60} allow the molecules to move apart more easily than atoms in a typical covalent crystal.

The thermal conductivity (κ) is very low (κ = 0.3 -0.6 W m^{-1} K^{-1}). This is comparable to that of amorphous materials and much lower than that of crystalline semiconductors. The low thermal conductivity can be attributed to the strong

phonon scattering process in the molecular crystal. Heat-carrying phonons are scattered by molecular rotation, orientation disorder, and weak intermolecular contacts, which leads to the lack of phonon mean free paths. In this sense, fullerite is an excellent thermal insulator despite its crystalline structure.

An important indicator of anharmonicity is the Grüneisen parameter (γ), which is about 1.8 to 2.4. Values larger than 1 indicate strong coupling between lattice vibrations and volume changes. The large values of γ show that phonon frequencies are strongly sensitive to pressure and temperature, which is indicative that fullerite is strongly anharmonic. This is not surprising, as it expands very fast and has a low thermal conductivity.

The temperature of the thermal stability or transformation is predicted to be close to 1200 K, which is in agreement with experiment. However, fullerite is not a simple melting agent. At much higher temperatures and pressure, neighboring C_{60} molecules form intermolecular covalent bonds and polymerize and transform naturally before melting. So the temperature is a transformation threshold rather than a melting point.

The pressure coefficient of melting (dT_m/dP) is estimated to be 250 to 400 K GPa^{-1}, which shows a strong increase in thermal stability under compression. This process is explained in terms of the Lindemann melting criterion, which relates melting to atomic vibrational amplitudes. The compression reduces the distance between the two molecules and increases the phonon frequencies. This reduces thermal vibrations and increases the transformation temperature. The pressure leads to stiffening of lattice structures from the thermodynamic point of view. The intermolecular van der Waals interactions become stronger, the bulk modulus increases, phonon frequencies move to higher energies, and anharmonic effects are lessened. As a result, fullerite thermal stability increases fast under compression, preventing structural changes and making it more resilient to thermal degradation.

3.7. Convergence Tests for Solid C_{60}:

Table 6 Convergence behavior of the total energy (ΔE), residual stress (Δσ), and relative lattice-parameter variation (Δa/a) of solid C_{60} (fullerite, face-centered cubic structure) as a function of plane-wave cutoff energy, evaluated using a fixed 2 × 2 × 2 Monkhorst–Pack k-point mesh. The small variations across all quantities confirm that the chosen cutoff energy ensures reliable convergence of total energy and structure.

Material	ΔE (meV/atom)	Δσ (GPa)	Δa/a (%)
C_{60} (Fullerite, fcc)	0.6	0.004	0.01

Table 6 shows the convergence of the calculated total energy (ΔE), residual stress (Δσ) and relative lattice parameter variation (Δa/a) for crystalline fullerite (fcc C_{60}) with respect to plane-wave cutoff energy. These quantities can be used to evaluate the numerical accuracy and reliability of density functional theory (DFT) calculations and to extract other physical quantities such as elastic constants, electronic structure and thermodynamic properties.

The total energy convergence criterion is of great importance because all ground-state properties are determined by it. The value of ΔE = 0.6 meV/atom is very small, so further changes in the plane-wave cutoff energy would not affect any of the calculated energies. Since variations below 1 meV/atom are generally considered fully converged in first-principles calculations, the chosen cutoff energy is highly accurate for fullerite.

The residual stress convergence is, of course, also critical for structural optimization. The stress variation is only Δσ = 0.004 GPa, and the internal stress tensor is essentially converged. This small value is several orders of magnitude smaller than the elastic constants of fullerite (C_{11} ≈ 24-26 GPa). The numerical errors associated with the incompleteness of a basis set are also negligible. The resulting structure is a real mechanical equilibrium.

The relative variation in lattice parameters is only Δa/a = 0.01%, thus crystal sizes are virtually unchanged with increasing cutoff energy. This is very important since the lattice parameters are what affect the equilibrium volume, density, and bulk modulus and fit equation of state. This very small variation confirms that the calculated structural properties are numerically stable and independent of the basis set.

Physically, the rapid convergence of fullerite is due to its molecular nature. The electronic states of C_{60} are mainly contained within fullerene cages and do not exhibit the highly oscillatory wavefunctions typical of transition metals or strongly correlated systems. A moderate plane-wave basis can be made to describe the electronic charge density.

Overall, the very small values of ΔE, Δσ, and Δa/a confirm that our cutoff energy provides a well-converged description of the fullerite crystal, and subsequent calculations of the structural, mechanical, electronic, optical, and thermal properties are free of any significant numerical errors.

Table 7 Convergence of the total energy per atom (ΔE) of solid C_{60} with increasing k-point density at a fixed plane-wave cutoff energy of 500 eV. Due to the large molecular unit cell of fullerite, Brillouin-zone sampling converges rapidly, and a 2 × 2 × 2 k-point mesh is sufficient for accurate first-principles calculations.

Material	1×1×1 ΔE (meV/atom)	2×2×2 ΔE (meV/atom)	3×3×3 ΔE (meV/atom)
C_{60} (Fullerite, fcc)	3.5	1.2	0

Table 7 shows the convergence behavior of the total energy per atom of crystalline fullerite (C_{60}) with increasing Brillouin-zone sampling density. The calculations were carried out with the same plane-wave cutoff energy of 500 eV and by systematically increasing the Monkhorst-Pack k-point mesh from 1×1×1 to 3×3×3. Convergence testing is a key step in first-principles calculations because it ensures that the structural, electronic, and mechanical properties are independent of numerical parameters and reflect the real physical behavior of the material.

The energy difference decreases significantly in the calculation from 3.5 meV/atom for the Γ-point only (1×1×1) calculation to 1.2 meV/atom for the 2×2×2 k-point mesh and finally to 0 meV/atom for the denser 3×3×3 mesh. The overall decrease in the total energy variation indicates that as the k-points are more dense, the integration of the Brillouin zones becomes more accurate. The convergence trend suggests that the electronic structure is being better described as more reciprocal-space sampling points are included in the calculation.

One important fact is that only 1.2 meV/atom energy difference between 2×2×2 and 3×3×3 meshes in the 2×2×2 mesh is very small. In density functional theory, an energy variation of less than 1-2 meV/atom is considered to be sufficient to reliably predict the equilibrium structures of the entire fullerite crystal, elastic constants, electronic band structure, and thermodynamic properties. The results imply that the 2×2×2 mesh already captures nearly all electronic information of the fullerite crystal and that further increases of k-point density do not lead to any enhancement in the accuracy.

The rapid convergence of fullerite can be explained by the unusual molecular-crystal properties of fullerite. Unlike conventional semiconductors or metallic systems, fullerite has a very large face-centered cubic unit cell with a lattice parameter of about 14 Å and four C_{60} molecules per unit cell. The large real-space dimensions correspond to a relatively small reciprocal-space Brillouin zone, and the electronic bands vary slowly with crystal momentum so that the k-point sampling is not required to be dense. Moreover, the semiconducting band gap of C_{60} removes the sharp electronic features near the Fermi level that usually require k-point sampling in metallic materials.

Another factor contributing to the rapid convergence is the weak intermolecular van der Waals interaction between neighboring fullerene molecules. Such interactions result in narrow electronic bandwidths and relatively flat valence and conduction bands, which indicate low electronic dispersion throughout reciprocal space. As a result, the total energy depends only weakly on the number of k-points, and the calculations can be performed with relatively coarse meshes.

Thus, the convergence analysis clearly shows that a 2×2×2 Monkhorst-Pack k-point mesh is sufficient for an accurate first-principles study of fullerite. The negligible energy difference with the denser 3×3×3 mesh confirms that the selected sampling is the best combination of computational efficiency and numerical accuracy. We can confidently use this k-point grid for the subsequent optimization of structure, elastic properties, electronic band structure, optical response, thermodynamic properties, and equation of state of crystalline C_{60}.

Table 8 shows the evolution of the bulk modulus (B), isothermal compressibility (κ), and softness index (S) of crystalline fullerene (C_{60}) under hydrostatic pressure from 0 to 25 GPa. These parameters provide insights into the pressure-induced mechanical response of fullerite and show how the molecular crystal transforms from a very compressible soft material to a stiffer structure upon compression.

At 0 GPa, fullerite has a bulk modulus of only 18.1 GPa, and it is therefore very compressible. This is because of the weak van der Waals interactions that hold neighboring C_{60} molecules together in the face-centered cubic crystal. Unlike covalent or ionic crystals where strong interatomic bonds can be compressed, fullerite is a molecular solid, and it can

be compressed relatively easily when pressure is high. Thus the isothermal compressibility is 5.52×10^{-2} GPa^{-1}, and the volume of the crystal changes rapidly even at moderate external pressure.

Table 8 Pressure-Dependent Mechanical Softness and Compressibility Indicators of Fullerene (C_{60}).

Pressure (GPa)	**Bulk Modulus B (GPa)**	**Compressibility κ_T (10^{-2} GPa^{-1})**	**Softness Index S (10^{-2} GPa^{-1})**
0	18.1	5.52	5.52
2	20.4	4.9	4.9
5	23.9	4.18	4.18
10	28.6	3.5	3.5
15	33.2	3.01	3.01
20	37.8	2.64	2.64
25	42.5	2.35	2.35

As pressure is increased from 0 to 25 GPa, the bulk modulus increases slowly from 18.1 GPa to 42.5 GPa. This monotonic increase has a dramatic pressure-induced stiffening effect. In fact, compression reduces the distance between neighboring fullerene cages and enhances van der Waals attraction and short-range electron-cloud repulsion. The molecules are closer together, so the crystal becomes more and more resistant to compression, leading to a significant stiffening effect. The bulk modulus at 25 GPa is more than twice its ambient pressure value, which shows the strong hardening of the molecular lattice.

We see a similar drop in the isothermal compressibility. The compressibility drops from 5.52×10^{-2} GPa^{-1} at ambient conditions to 2.35×10^{-2} GPa^{-1} at 25 GPa. Since the compressibility is inversely proportional to the bulk modulus:

$$\kappa_T = \frac{1}{B} \tag{3}$$

The decrease in κ' was driven by the increase in the crystal's resistance to volume reduction under pressure. The decrease in compressibility indicates that fullerite becomes increasingly difficult to compress as more intermolecular interactions occur. The softness index (S) is similar to compressibility in that it is also inversely related to the material's resistance to deformation. For ambient pressure, the softness index is 5.52×10^{-2} GPa^{-1}. The very compliant nature of fullerite cannot be explained by temperature. As pressure increases, the softness falls to 2.35×10^{-2} GPa^{-1} at 25 GPa. The decrease indicates that a soft molecular crystal has been changed to a much more rigid and compact crystal.

In microscopic terms, this is because of the unique intermolecular potential for C_{60} crystals. At low pressures, the potential energy landscape is shallow as the intermolecular forces are dominated by weak dispersion interactions. When the intermolecular potential is compressed more compactly, the repulsive part of the potential increases very quickly due to the overlap of the electronic charge densities between adjacent fullerene cages. The high repulsion of the intermolecular potential leads to a sharp increase in rigidity of the lattice and a sharp decrease in softness.

The pressure dependence shown in Table 8 also confirms that no mechanical instability exists in the pressure range studied. The smooth increase in bulk modulus and the continuous decrease in compressibility indicate that the fullerite structure is stable under compression. The lack of abrupt changes would indicate that there is no pressure-induced structural phase transition below 25 GPa; however, significant electronic and vibrational changes might still occur with smaller intermolecular spacing.

Overall, the results indicate that fullerite is very sensitive to pressure, as molecular crystals dominated by van der Waals interactions are. While the material is very soft and compressible at ambient conditions, external pressure significantly enhances the intermolecular coupling, resulting in more robust lattice stiffness, less compressibility, and mechanical stability.

3.8. Determination of HOMO–LUMO Gap of C_{60} Under Pressure:

Table 9 Pressure-dependent variation of HOMO (E_{HOMO}), LUMO (E_{LUMO}), and HOMO–LUMO energy gap (Eg) of fullerene (C_{60}) calculated using density functional theory (DFT) within the pressure range of 0–25 GPa.

Pressure P (GPa)	E_{HOMO} (eV)	E_{LUMO} (eV)	Eg (eV)
0	−5.86	−3.62	2.24
5	−5.88	−3.78	2.1
10	−5.90	−3.92	1.98
15	−5.93	−4.05	1.88
20	−5.95	−4.16	1.79
25	−5.98	−4.26	1.72

Table 9 shows the pressure dependence of the highest occupied molecular orbital (HOMO), the lowest unoccupied molecular orbital (LUMO), and the HOMO-LUMO energy gap (Eg) of fullerene (C_{60}) at a pressure of 0- 25 GPa. These are the most important parameters in the electronic structure as they determine the charge transfer, optical absorption, electrical conductivity and chemical reactivity. The evolution of these quantities under pressure provides important information on the intermolecular electronic interactions and orbital hybridization in compressed fullerene.

At 0 GPa, the HOMO energy is -5.86 eV, and the LUMO energy is -3.62 eV. This corresponds to a gap of 2.24 eV between the HOMO and LUMO energies. This gap is similar to the semiconducting nature of C_{60} and is due to its very symmetric icosahedral molecular structure. The HOMO energy is mainly due to the occupied π bonding molecular orbitals of carbon 2p electrons, while the LUMO is due to the antibonding π* orbitals. These molecular orbitals are electron acceptors of light, and the large energy difference between the two orbitals is a result of the chemical stability of fullerene and that it is well suited to be an electron acceptor in photovoltaic and molecular electronics applications.

As pressure increases, the HOMO and LUMO energies change to lower energies, implying that the electronic states are gradually stabilized. The HOMO decreases from -5.86 eV at ambient conditions to -5.98 eV at 25 GPa, while the LUMO decreases from -3.62 eV to -4.26 eV. The higher pressure dependence of the LUMO suggests that the unoccupied antibonding states are more sensitive to intermolecular interactions than the occupied bonding states. This is because compression reduces the distance between the neighboring fullerene molecules, which causes orbital overlap and thus the electronic coupling throughout the crystal.

One of the consequences of pressure-induced orbital interactions is that the HOMO-LUMO energy gap decreases systematically from 2.24 eV at 0 GPa to 1.72 eV at 25 GPa, a loss of approximately 23%. This drop in energy gap indicates that the electronic structure becomes more and more conductive with the compression. The more closely the molecular orbitals are together, the broader the electronic bands are, and the more the occupied and unoccupied states are separated. The energy needed to excite a HOMO electron to the LUMO is therefore less.

The reduction of the energy gap can also be understood from a molecular orbital view. In compression, the fullerene cages approach each other and strengthen the intermolecular π–π interactions. This increases the dispersion of both the valence and conduction bands, and causes the LUMO to slope downward in comparison to the HOMO. The conduction-band states are more delocalized and spatially extended. These are much more affected by pressure than the valence-band states. Consequently, the conduction-band edge moves closer to the valence-band edge, and the band gap narrows.

From an optical point of view, the decreasing HOMO–LUMO gap induces a redshift of the optical absorption edge with increasing pressure. These lower-energy photons are sufficient to induce electronic excitations, and thus enhance visible light absorption. This is especially relevant in optoelectronic applications where pressure can be used as a tuning parameter to tune the electronic and optical response of fullerene-based materials.

The smooth and continuous variation of EHOMO, ELUMO, and Eg throughout the studied pressure range indicates that the electronic phase transition does not occur abruptly at 25 GPa. The electronic structure gradually moves from a wider-gap molecular semiconductor to a narrower-gap semiconducting one. The existence of a finite range of energy

gap at 25 GPa suggests that fullerene is still semiconducting in the pressure range studied, although its electrical conductivity will improve.

Overall, our results show that external pressure is useful for tuning the electronic properties of fullerene. The downward shift in molecular orbital energies and the narrowing of the HOMO-LUMO gap are indicative of increased intermolecular electronic coupling and orbital delocalization when compressed. Such changes in fullerene are very important in designing electronic, photovoltaic, sensing and energy storage devices.

3.9. Pressure-Dependent Electronegativity and Electrophilicity Index:

Table 10 Pressure-dependent variation of chemical potential (μ), electronic hardness (η), electronegativity (χ), and electrophilicity index (ω) of fullerene (C_{60}) calculated using density functional theory (DFT) in the pressure range of 0–25 GPa.

Pressure (GPa)	μ (eV)	ρ (eV)	χ = −μ (eV)	ω (eV)
0	−4.74	1.12	4.74	10.02
5	−4.83	1.05	4.83	11.11
10	−4.91	0.99	4.91	12.17
15	−4.99	0.94	4.99	13.25
20	−5.06	0.9	5.06	14.28
25	−5.12	0.86	5.12	15.24

Table 10 summarizes the variation of the chemical potential (μ), electronic hardness (η), electronegativity (χ), and electrophilicity index (ω) of fullerene (C_{60}) under hydrostatic pressure (0, 25 GPa). These DFT descriptors give an insight into the electronic stability, charge acceptability, and chemical reactivity of the molecule under compression. Their evolution under pressure is an indication of the change of electronic structure and chemical nature of fullerene in the presence of external pressure.

At 0 GPa, the chemical potential is -4.74 eV, which means that electrons are most likely to stay in the fullerene cage. As pressure increases to 25 GPa, μ slowly decreases to -5.12 eV. The negative chemical potential indicates electronic stabilization under compression. Physically, pressure leads to a decrease in distances between molecules and an increase in orbital overlap of neighboring C_{60} molecules, so the electronic states become less stable at lower energies.

The electronic hardness (η) measures the resistance of a system to charge transfer or electronic deformation and decreases systematically from 1.12 eV at ambient pressure to 0.86 eV at 25 GPa. In this conceptual DFT, hardness is directly related to the HOMO-LUMO gap through $\eta \approx Eg/2$. The decrease in hardness is therefore consistent with the pressure-induced narrowing of the energy gap in Table 9. The smaller hardness is also indicative that electrons can be redistributed more easily under external perturbations, indicating that compressed fullerene becomes more chemically reactive and electronically polarizable.

The electronegativity (χ), i.e., the negative of the chemical potential ($\chi = -\mu$), increases continuously from 4.74 eV to 5.12 eV as pressure rises. The increase in electronegativity indicates that fullerene has an even stronger tendency to accept electrons under compression. The higher electronegativity is due to the downward shift of the HOMO and LUMO energy levels, which makes the molecule more capable of accepting electrons. This is particularly important for applications in charge transfer such as organic photovoltaics, molecular electronics, and electron transport.

One of the most notable changes in the electrophilicity index (ω) increases sharply from 10.02 eV at 0 GPa to 15.24 eV at 25 GPa. As electrophilicity is defined as $\omega = \mu^2/2\eta$, its increase occurs simultaneously with the decrease of hardness and increase in electronegativity. The larger ω values indicate that fullerene becomes a stronger electron acceptor under pressure. This is because the electrophilic character is more susceptible to charge transfer and electrophilic chemical processes.

In the end, we found that hydrostatic pressure greatly changes the electronic reactivity of C_{60}. In addition, compression makes the electronic structure stronger, less hard to work with, electronegativity is stronger, and electrophilicity is much higher. These changes indicate that pressure increases charge transfer and electron delocalization, making

fullerene more reactive and a more effective electron acceptor. Such pressure-tuned electronic properties are very important for the development of new fullerene-based materials for energy storage, molecular sensing, organic electronics, photocatalysis, and photovoltaic applications.

3.10. Universal elastic anisotropy index of C_{60} at 0 GPa:

Table 11 Voigt and Reuss estimates of the bulk and shear moduli, together with the calculated Universal Elastic Anisotropy Index (A^U), for C_{60} at ambient pressure (0 GPa).

Material	Pressure (GPa)	B_v (GPa)	B^R (GPa)	G_v (GPa)	G^R (GPa)	A^U
C_{60} (Fullerene)	0	18.5	17.9	7.8	7.4	0.12

Table 11 provides Voigt and Reuss estimates for the bulk modulus (B_v) and shear modulus (G_v) and the calculated Universal Elastic Anisotropy Index (A^U) for crystalline fullerene (C_{60}) at ambient pressure. These parameters are important to determine the elastic uniformity of the material and the direction of mechanical properties. The elastic anisotropy is a very important property as it affects deformation, crack propagation, thermal stress distribution, and mechanical stability under external loads.

The Voigt approximation assumes uniform strain throughout the crystal and is generally the upper limit of elastic moduli. For fullerite the Voigt bulk modulus is 18.5 GPa and the shear modulus is 7.8 GPa. These values indicate the best possible effective resistance of the crystal to volumetric and shear deformation if all crystallographic directions are subjected to the same strain. On the other hand, the Reuss approximation considers the same stress throughout the material and finds the lower limit of elastic moduli.

For the bulk modulus B^R = 17.9 GPa and the shear modulus G^R = 7.4 GPa calculated by Reuss, the Voigt and Reuss estimates are only slightly different. The small difference between Voigt and Reuss's estimates indicates that the elastic response of fullerite is almost homogeneous in all crystallographic directions. Physically, this is due to the very symmetric face-centered cubic shape of C_{60} molecules and the almost isotropic distribution of intermolecular van der Waals interactions in the crystal lattice.

The close agreement between the Voigt and Reuss bounds is important, as large differences usually indicate strong directional dependence of elastic properties. In fullerite, however, the differences are only 0.6 GPa for the bulk modulus and 0.4 GPa for the shear modulus. Such small deviations imply that compression and shear deformation are distributed fairly uniformly throughout the crystal structure. This mechanical uniformity is the direct consequence of the high molecular symmetry of the C_{60} cage and the cubic symmetry of the fullerite lattice.

A more quantitative measure of anisotropy is the Universal Elastic Anisotropy Index (A^U). For an elastically isotropic material, A^U = 0, and larger values correspond to increasing anisotropy. We found that fullerene has A^U = 0.12, and this is very close to zero. This extremely small value corresponds to fullerite being almost isotropic in its structure. In other words, its mechanical properties are totally independent of the direction of crystallography, and it reacts to an applied stress in the same way irrespective of the direction.

In principle, the low anisotropy is due to the spherical C_{60} molecules spreading stress in the crystal. Unlike layered materials such as graphite or anisotropic crystals such as black phosphorus, where bonding strength is very different in different directions, fullerite has a three-dimensional molecular packing arrangement with relatively uniform intermolecular interactions. Deformation is thus almost isotropic.

The low elastic anisotropy also has practical implications. Materials with small anisotropy have a more uniform mechanical performance and thus less susceptibility to directional cracking and better structural reliability. So the anisotropy index calculated suggests fullerite can maintain stable mechanical performance in multidirectional loading and pressure regimes.

The results of Table 11 are clear that crystalline C_{60} is a mechanically soft but elastically isotropic molecular crystal. The excellent agreement of Voigt and Reuss moduli with a very small Universal Elastic Anisotropy Index indicates that the fullerite lattice is very uniform in elasticity despite the weak van der Waals interaction.

4. Conclusion

In this work, we have conducted a detailed density functional theory (DFT) analysis of the crystalline fullerene (C_{60}) in its FCC phase to elucidate its structure and mechanical, electronic, optical, and thermal properties at pressures ranging from 0 to 25 GPa. Our equilibrium structure model values, comprising lattice constant, unit cell volume, density, and intermolecular separation, were in good agreement with experimental data for van der Waals interactions, providing evidence of the crucial role of dispersion forces in the description of molecular crystals. The Birch-Murnaghan equation-of-state fit yielded an equilibrium volume of $\sim$ 2845 $Å^3$ and a bulk modulus of $\sim$ 18.1 GPa, indicating that fullerite is highly compressible at room temperature.

The elastic constants are maintained to Born stability over the pressure range, and the FCC phase is mechanically stable. The low bulk, shear, and Young's moduli show weak intermolecular van der Waals forces, while the Pugh ratio and Poisson's ratio show moderate ductility and elastic flexibility. The small Universal Elastic Anisotropy Index (A^U = 0.12) also shows that fullerite is nearly isotropic in mechanical behavior. The bulk modulus and compressibility are significantly enhanced over the pressure range, implying that the lattice is progressively stiffened under compression.

Electronic structure analysis showed that fullerene remains semiconducting across the pressure range. With increasing pressure, HOMO and LUMO energy levels shift to lower energies while the gap between HOMO and LUMO decreases from 2.24 eV at ambient pressure to 1.72 eV at 25 GPa. With increasing pressure, the band gap is reduced due to intermolecular overlap and electronic delocalization. Conceptual DFT descriptors indicate that the electronegativity and electrophilicity of fullerene increase with increasing pressure, and the electronic hardness decreases. That is, compressed fullerene is a stronger electron acceptor and reacts more easily.

The optical properties verified the dominance of π–π* electronic transitions, and the dielectric constants, refractive index, optical conductivity, and absorption spectra were in good agreement with experiments. Thermal analysis showed a very high specific heat capacity, low Debye temperature, large thermal expansion, and low thermal conductivity as a result of the soft and anharmonic nature of the molecular crystal. Moreover, pressure was found to greatly enhance the thermal stability through stiffening the lattice and suppressing the anharmonic lattice vibration.

As a whole, we have shown that external pressure can be used to tune the mechanical rigidity, electronic structure, optical properties, and chemical reactivity of fullerene. The results also provide us with a picture of the fundamental physics of molecular crystals, and it is a promising material for molecular electronics, organic photovoltaics, energy storage, sensors, and pressure-responsive nanodevices.

Compliance with ethical standards

Statement of ethical approval

The authors confirm that it is their original work and has not been submitted elsewhere or published.

Author's Contribution

Mr. Sourabh Kumar Srivastava and Mr. Mohammad Tauseef Raza made an original draft of the manuscript under the supervision of Dr. Raj Kumar Singh and Purshottam Kumar Srivastava.

Availability of data and Materials

Data made available at request.

References

[1] Abhay P. Srivastava, Brijesh K. Pandey, Pressure-dependent structural, mechanical, and thermal properties of magnesiowüstite: A DFT and EOS study, International Journal of Modern Physics B, 40(04), 2650024 (2026), https://doi.org/10.1142/S0217979226500244.

[2] Nangamso Nathaniel Nyangiwe, Applications of density functional theory and machine learning in nanomaterials: A review, Next Materials, 8,2025,100683, https://doi.org/10.1016/j.nxmate.2025.100683.

[3] Muniz-Miranda, F.; Pedone, A.; Menziani, M.C.; Muniz-Miranda, M. DFT and TD-DFT Study of the Chemical Effect in the SERS Spectra of Piperidine Adsorbed on Silver Colloidal Nanoparticles. Nanomaterials 2022, 12, 2907. https://doi.org/10.3390/nano12172907.

[4] Abhay P. Srivastava, Brijesh K. Pandey, Enhancing the optoelectronic performance of ABX3 perovskites (A=MA+/FA+, B=Pb2+, X=I−/Br−): A comprehensive first-principles investigation for next-generation solar cell technology, International Journal of Modern Physics B, https://doi.org/10.1142/S0217979225502923.

[5] Obijiofor, O.C., Novikov, A.S. Exploring the role of density functional theory in the design of gold nanoparticles for targeted drug delivery: a systematic review. J Mol Model 31, 186 (2025). https://doi.org/10.1007/s00894-025-06405-9.

[6] Madhulata Shukla, Alkadevi Verma, Sunil Kumar, Shaili Pal, Indrajit Sinha, Experimental and DFT calculation study of interaction between silver nanoparticle and 1-butyl-3-methyl imidazolium tetrafluoroborate ionic liquid, Heliyon, 7(1), 2021, e06065, https://doi.org/10.1016/j.heliyon.2021.e06065.

[7] Maurya, D., Pandey, B.K. & Srivastava, A.P. Mechanically robust and optically active Mg80Ni10Nd10 metallic glass: first-principles evidence for next-generation optical coatings. Opt Quant Electron 58, 28 (2026). https://doi.org/10.1007/s11082-025-08615-0.

[8] Hashemkhani Shahnazari, G., Darvish Ganji, M. Understanding structural and molecular properties of complexes of nucleobases and Au13 golden nanocluster by DFT calculations and DFT-MD simulation. Sci Rep 11, 435 (2021). https://doi.org/10.1038/s41598-020-80161-z.

[9] Michos, F.I.; Papaspiropoulou, C.; Aravantinos-Zafiris, N.; Sigalas, M.M. Optical and Vibrational Properties of AlN Nanoparticles with Different Geometries: A DFT and TD-DFT Study. Crystals 2025, 15, 1003. https://doi.org/10.3390/cryst15121003.

[10] Srivastava, A. Prakash, Pandey, B. Kumar, and Shanker, A. (2025). Pressure-Dependent Structural, Mechanical, and Thermal Behavior of $Zr_{50.5}Ti_{4.8}Cu_{19.0}Ni_{11.4}Al_{14.3}$ Bulk Metallic Glass: A DFT and Equation of State Study. (e234974). Physical Chemistry Research (14), e234974. https://doi.org/10.22036/pcr.2025.552725.2766.

[11] Kubicki, J.D., Kabengi, N., Chrysochoou, M. et al. Density functional theory modeling of chromate adsorption onto ferrihydrite nanoparticles. Geochem Trans 19, 8 (2018). https://doi.org/10.1186/s12932-018-0053-8.

[12] Srivastava, A.P., Pandey, B.K. First-principles and equation of state investigation of pressure-tunable structural, mechanical, thermodynamic, and electronic properties of high-reflecting nano-metal oxides: insights into high-performance optoelectronic and energy applications. Appl Nanosci 15, 47 (2025). https://doi.org/10.1007/s13204-025-03124-8.

[13] Ataei, S., Nemati-Kande, E. & Bahrami, A. Quantum DFT studies on the drug delivery of favipiravir using pristine and functionalized chitosan nanoparticles. Sci Rep 13, 21984 (2023). https://doi.org/10.1038/s41598-023-49298-5.

[14] Selli, D.; Fazio, G.; Di Valentin, C. Using Density Functional Theory to Model Realistic TiO2 Nanoparticles, Their Photoactivation and Interaction with Water. Catalysts 2017, 7, 357. https://doi.org/10.3390/catal7120357.

[15] Abhay P. Srivastava and Brijesh K. Pandey, Atomic-Level Design of Doped TiO2 for Enhanced Lithium Storage: A Density Functional Theory Approach, 2025 J. Electrochem. Soc. 172 113502, https://doi.org/10.1149/1945-7111/ae1be1.

[16] Shafaei, A., Khayati, G. R., & Hoshyar, R. (2023). Green and cost-effective synthesis, characterization, and DFT study of silver nanoparticles for improving their biological properties by opium syrup as a biomedical drug and good biocompatibility. Inorganic and Nano-Metal Chemistry, 53(12), 1343–1357. https://doi.org/10.1080/24701556.2021.1993257.

[17] Srivastava, A. Prakash, and Pandey, B. Kumar (2026). A Computational Study of Pressure-Induced Melting in $LaFeO_3$: Using DFT and Semi-Empirical Model. Physical Chemistry Research, 14(1), 1- 7. https://doi.org/10.22036/pcr.2025.537079.2712.

[18] Srivastava, A.P., Pandey, B.K. Studying the Melting Behavior of Fullerene by Utilizing the Equation of State and Lindemann's Law. Natl. Acad. Sci. Lett. (2025). https://doi.org/10.1007/s40009-025-01782-4.

[19] Negi, A., Ringwal, S., Pandey, M. et al. Plant-mediated Z-scheme ZnO/TiO2-NCs for antibacterial potential and dye degradation: experimental and DFT study. Sci Rep 14, 7955 (2024). https://doi.org/10.1038/s41598-024-57392-5.

[20] Abbasi, A., Sardroodi, J.J. Molecular design of O3 and NO2 sensor devices based on a novel heterostructured N-doped TiO2/ZnO nanocomposite: a van der Waals corrected DFT study. J Nanostruct Chem 7, 345–358 (2017). https://doi.org/10.1007/s40097-017-0244-3.

[21] Gunasekaran, A.; Rajamani, A.K.; Masilamani, C.; Chinnappan, I.; Ramamoorthy, U.; Kaviyarasu, K. Synthesis and Characterization of ZnO Doped TiO2 Nanocomposites for Their Potential Photocatalytic and Antimicrobial Applications. Catalysts 2023, 13, 215. https://doi.org/10.3390/catal13020215.

[22] Abhay P. Srivastava, Brijesh K. Pandey, Pressure-dependent evolution of Bi2Sr2CaCu2O8+δ: DFT insights for high-pressure superconducting applications, Solid State Communications, 404, 2025, 116112, https://doi.org/10.1016/j.ssc.2025.116112.

[23] Srivastava, A. Prakash, Pandey, B. Kumar, Singh, A. Kumar, Srivastava, R. and Srivastava, H. Chandra (2025). Assessment of Several Equations of State for the Calculation of Thermodynamic Coefficients of Solids. Physical Chemistry Research, 13(4), 669-676. doi: 10.22036/pcr.2025.524577.2685.

[24] Sahni, V. (2004). The Hohenberg-Kohn Theorems and Kohn-Sham Density Functional Theory. In: Quantal Density Functional Theory. Springer, Berlin, Heidelberg. https://doi.org/10.1007/978-3-662-09624-6_4.

[25] Wang, P.; Hu, D.; Lu, L.; Zhao, Y.; Chen, J.; Ayers, P.W.; Liu, S.; Zhao, D. Predicting the Post-Hartree-Fock Electron Correlation Energy of Complex Systems with the Information-Theoretic Approach. Molecules 2025, 30, 3500. https://doi.org/10.3390/molecules30173500.

[26] Däne, M.; Gonis, A. On the v-Representability Problem in Density Functional Theory: Application to Non-Interacting Systems. Computation 2016, 4, 24. https://doi.org/10.3390/computation4030024.

[27] Itas, Y.S.; Suleiman, A.B.; Ndikilar, C.E.; Lawal, A.; Razali, R.; Khandaker, M.U.; Ahmad, P.; Tamam, N.; Sulieman, A. The Exchange-Correlation Effects on the Electronic Bands of Hybrid Armchair Single-Walled Carbon Boron Nitride Nanostructure. Crystals 2022, 12, 394. https://doi.org/10.3390/cryst12030394.

[28] Abhay P. Srivastava, Brijesh K. Pandey, Analysis of the Structural and Electronic Properties of TiO2 Under Pressure Using Density Functional Theory and Equation of State, Computational Condensed Matter, 2025,e01076, https://doi.org/10.1016/j.cocom.2025.e01076.

[29] Abhay. P. Srivastava, B.K. Pandey, A. K., Gupta, et al. A New Approach to Evaluate Pressure of Solids at High Compression. Natl. Acad. Sci. Lett. 47, 713–718 (2024). https://doi.org/10.1007/s40009-024-01409-0.

[30] Dincer, I.; Cengel, Y.A. Energy, Entropy and Exergy Concepts and Their Roles in Thermal Engineering. Entropy 2001, 3, 116-149. https://doi.org/10.3390/e3030116.

[31] Srivastava, A. Prakash, Pandey, B. Kumar, Singh, A. Kumar, Srivastava, R. and Srivastava, H. Chandra (2025). Assessment of Several Equations of State for the Calculation of Thermodynamic Coefficients of Solids. Physical Chemistry Research, 13(4), 669-676. doi: 10.22036/pcr.2025.524577.2685.

[32] Umrigar, C.J., Savin, A., Gonze, X. (1998). Are Unoccupied Kohn-Sham Eigenvalues Related to Excitation Energies?. In: Dobson, J.F., Vignale, G., Das, M.P. (eds) Electronic Density Functional Theory. Springer, Boston, MA. https://doi.org/10.1007/978-1-4899-0316-7_12.

[33] ALLEN, M. J., & TOZER, D. J. (2002). Eigenvalues, integer discontinuities and NMR shielding constants in Kohn—Sham theory. Molecular Physics, 100(4), 433–439. https://doi.org/10.1080/00268970110078335.

[34] Abhay. P. Srivastava, B.K. Pandey, A. K., Gupta, et al. A New Approach to Evaluate Pressure of Solids at High Compression. Natl. Acad. Sci. Lett. 47, 713–718 (2024). https://doi.org/10.1007/s40009-024-01409-0.

[35] Abhay. P. Srivastava, B.K. Pandey, A. K. Gupta, et al. Theoretical prediction of thermoelastic properties of bismuth ferrite by a new approach. J Math Chem 62, 2253–2264 (2024). https://doi.org/10.1007/s10910-024-01647-z.

[36] Abhay. P. Srivastava, B.K. Pandey, A. K. Gupta, et al. The Relevance of the New Exponential Equation of State for Semiconductors. Iranian Journal of Science, 48, 1067–1074 (2024). https://doi.org/10.1007/s40995-024-01657-1.

[37] Abhay P. Srivastava, Brijesh K. Pandey, Abhishek Kumar Gupta, Calculation of the melting curve of metals using equations of state and Lindemann's law, Computational Condensed Matter, 42, 2025, e00986, https://doi.org/10.1016/j.cocom.2024.e00986.

[38] Abhay P. Srivastava, Brijesh K. Pandey, Abhishek K. Gupta, Explore the fascinating realm of comparing metal melting curves by applying the equation of state and Lindemann's law, Computational Condensed Matter, 40, 2024, e00952, 2352-2143, https://doi.org/10.1016/j.cocom.2024.e00952.

[39] Nye, J. F. Physical Properties of Crystals, Oxford University Press.

[40] Anderson, O. L. (1995). Equations of state of solids for geophysics and ceramic science. Oxford University Press.

[41] Abhay. P. Srivastava, B.K. Pandey, A. K. Gupta, et al. Comparing Melting Curves of Metals Using the Equation of State and Lindemann's Law. Iran J Sci (2024). https://doi.org/10.1007/s40995-024-01748-z.

[42] Abhay. P. Srivastava, B.K. Pandey, A constructive approach to formulating pressure-dependent binding energy using the equation of state. Ionics (2025). https://doi.org/10.1007/s11581-025-06183-7.

[43] Abhay. P. Srivastava, B. K. Pandey, & M. Upadhyay, (2024). Anticipating Pressure Changes in Halides under Compression. East European Journal of Physics, (3), 333-339. https://doi.org/10.26565/2312-4334-2024-3-37.

[44] Abhay P. Srivastava, Brijesh K. Pandey, Anod Kumar Singh, Reetesh Srivastava, A New Fourth Order Compression Dependent Equation of State, East European Journal of Physics (2025)1, 332-339, https://doi.org/10.26565/2312-4334-2025-1-40.

[45] P. A. Heiney, J. E. Fischer, A. R. McGhie, W. A. Romanow, and A. M. Denenstein, J. P. McCauley, Jr., A. B. Smith, III, D. E. Cox, Heiney et al. reply, Phys. Rev. Lett. 67, 1468, 1991, https://doi.org/10.1103/PhysRevLett.67.1468.

[46] Steven J. Duclos, Keith Brister, R. C. Haddon, A. R. Kortan, F. A. Thiel, Effects of pressure and stress on C60 fullerite to 20 GPa. Nature 351, 380–382 (1991). https://doi.org/10.1038/351380a0.

[47] H. W. Kroto, J. R. Heath, S. C. O'Brien, R. F. Curl, R. E. Smalley, C60: Buckminsterfullerene. Nature 318, 162–163 (1985), https://doi.org/10.1038/318162a0.

[48] John E. Fischer, Paul A. Heiney, Amos B. Smith, III, Solid-state chemistry of fullerene-based materials, Acc. Chem. Res. 1992, 25, 3, 112–118, https://doi.org/10.1021/ar00015a003.

[49] Hsiao-Chi Lu,‹ Meng-Yeh Lin, Yu-Chain Peng, Sheng-Lung Chou, Jen-Iu Lo, Bing-Ming Cheng, Absorption, emission and photolysis of C60 with far-UV excitation, MNRAS452, 2788–2793 (2015), https://doi.org/10.1093/mnras/stv1460.

[50] Haddon, R. C., Perel, A. S., Morris, R. C., Palstra, T. T. M., Hebard, A. F., & Fleming, R. M. (1995). C-60 thin-film transistors. Applied Physics Letters, 67(1), 121- 123. https://doi.org/10.1063/1.115503.

[51] M. Knupfer, J.F. Armbruster, H.A. Romberg, J. Fink, Electronic structure of K: C60 compounds studied using electron energy-loss spectroscopy, Synthetic Metals, 70(1–3), 1995, 1321-1324, https://doi.org/10.1016/0379-6779(94)02865-V.

[52] K. Tanigaki, I. Hirosawa, T. Manako, J. S. Tsai, J. Mizuki, T. W. Ebbesen, Phase transitions in Na2AC60 (A=Cs, Rb, and K) fullerides, Phys. Rev. B 49, 12307, 1994, https://doi.org/10.1103/PhysRevB.49.12307.

[53] Meletov, K.P., Maksimov, A.A. & Tartakovskii, I.I. Energy spectrum and phase transitions in C70 fullerite crystals at high pressure. J. Exp. Theor. Phys. 84, 144–150 (1997). https://doi.org/10.1134/1.558143.

[54] Tareyeva, E.E., Schelkacheva, T.I. & Chtchelkatchev, N.M. Orientation ordering and the transition to the orientational glass state in fullerite C60. Theor Math Phys 155, 812–823 (2008). https://doi.org/10.1007/s11232-008-0070-3.

[55] R. Moret, P. Launois, P.-A. Persson and B. Sundqvist, First X-ray diffraction analysis of pressure polymerized C60 single crystals, 1997 EPL 40 55, https://doi.org/10.1209/epl/i1997-00424-4.